Acta Cryst. (1969). A25, 595

Multiple-Beam Dynamic Effects in Kikuchi Patterns from Natural Spinel

BY J. GJØNNES AND R. HØIER

Department of Physics, University of Oslo, Norway

(*Received* 28 *October* 1968)

Transmission Kikuchi line patterns from wedge-shaped crystals of natural spinel have been studied. Especially near line intersections, extensive contrast anomalies attributable to multiple-beam interactions were observed, such as enhanced and diminished line segments, split lines and line segments which can not be indexed as ordinary Kikuchi lines. Several effects sometimes combine to form extensive patterns related to the Kikuchi envelope. The observed patterns are compared with calculated line contrast using several interacting beams. Most of the effects can be explained through three interacting beams; hence, three-beam effects in Kikuchi patterns are discussed in some detail. General rules for the dependence of contrast anomalies on signs and sizes of the Fourier potentials are derived. It is pointed out that, because of the wide range of diffraction conditions recorded in one exposure and the elimination of thickness-dependent oscillations, Kikuchi patterns give a very useful picture of the angular extent of the most important dynamic interactions. Applications of the results in connection with other diffraction techniques are discussed.

Introduction

Kikuchi patterns are of considerable interest to the electron diffractionist. They can be used for accurate determination of crystal orientation and lattice constants (Uyeda, 1965; Høier, 1969); also, they represent an interesting diffraction phenomenon which may yield insight into dynamic interactions as well as into the nature of diffuse scattering (see *e.g.* Gjønnes, 1966).

Hence, a detailed understanding of the deviations of position and contrast of Kikuchi lines from the predictions of simple theory – geometrical or two beam – is desirable. Such deviations have been reported by several investigators (Shinohara, 1932; Pfister, 1953; Menzel-Kopp, 1962; Gjønnes & Watanabe, 1966) and are to a large extent recognized as arising from multiple beam interactions. In fact, Shinohara (1932) had already introduced three-beam considerations in order to explain the Kikuchi envelope. Very recently, Watanabe, Uyeda & Fukuhara (1968) have demonstrated how multiple-beam effects in Kikuchi patterns can be used to obtain accurate values for Fourier potentials.

Whereas multiple beam interactions in spot patterns and in convergent beam patterns have been studied in considerable detail, less effort appears to have been put into theoretical explanation of contrast details in Kikuchi patterns, despite the considerable simplification in calculation procedure one may gain from the thickness average inherent in Kikuchi line contrast.

The aim of the present work has been to explain, through multiple-beam calculations, various effects observed in Kikuchi patterns from single crystals of natural spinel. The emphasis has been on typical contrast anomalies resulting from multiple-beam interactions and on the relationship between contrast effects in the different regions coupled through such interactions. Spinel was chosen as the material partly because it permitted a study of the effect of the signs of structure factors.

Experimental results

Kikuchi patterns from small chips of natural spinel, $MgAl_2O_4$, were obtained in the selected area position using a JEM 7 electron microscope. A variety of multiple-beam effects were recognized in the patterns, such as anomalies in line contrast and position; black and white dots at the lines; split spots at line intersections; displaced line segments. The various effects often combine to form complicated curved figures, of which the envelope can be seen as one example.

Enhanced or diminished contrast at certain segments of a Kikuchi line is a frequently occurring anomaly, typical examples of which are shown in Fig. 1. The excess line $7\bar{3}1$ appears with almost vanishing contrast in the corner outside the excess lines $2\bar{4}2$ and 511.* Similar contrast changes are seen on the $9\bar{7}3$ excess line. The vanishing of contrast under rather similar conditions was studied by Pfister (1953) and Menzel-Kopp (1962) who formulated a rule for the contrast changes in terms of angles between the scattering vectors operating. The contrast changes in Fig. 1 are consistent with this rule.

Inside the 511 line there is strong enhancement of contrast of the $7\bar{3}1$ and $9\bar{7}3$ lines, particularly near to their intersections with 511. Here the $7\bar{3}1$ line is split, with small tails pointing approximately in the direction of the $2\bar{4}2$ line. At the corresponding place on the $2\bar{4}2$ line, *viz.* at the $5\bar{1}1$, $2\bar{4}2$ intersection, this line is also split. Similar gaps and enhanced spots were observed at a number of line intersections.

* 'Outside the line' here refers to that side of the line which is opposite to the other line of the pair. Similarly 'inside a line' refers to the side which is between the two lines of a pair.

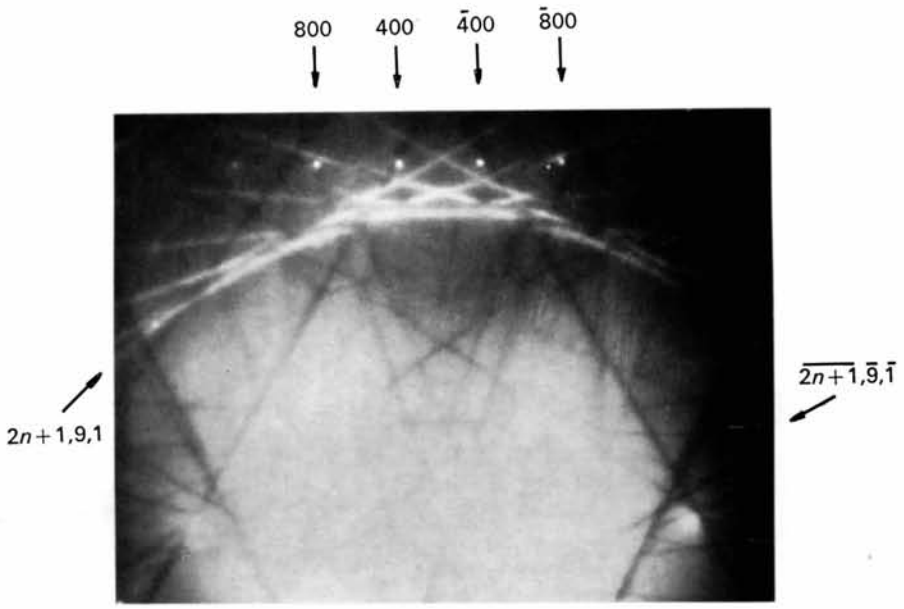

Fig.4. Transmission Kikuchi pattern showing the $\pm(2n+1,9,1)$ envelopes.

[*To face p.* 595

A more complicated pattern is reproduced in Fig. 2, where the dominant lines belong to the [01$\bar{2}$] zone. The features to be discussed are shown in Fig. 3. There are several enhanced segments, notably on the $\pm(4n+2,4,2)$ lines, *e.g.* on the $\overline{642}$ excess line outside $\bar{4}00$ and $\overline{242}$. Inside these lines the contrast of $\overline{642}$ is reduced. Along the ± 242 lines there are contrast anomalies changing from enhancement to reduction at several intersections. Starting from the left in Fig. 2, the $\overline{242}$ excess line contrast is enhanced outside 400, reduced immediately inside this line, enhanced again on approaching $\overline{242}$ and reduced inside the $\overline{242}$ line. Similar contrast changes are seen along the corresponding deficient line. These contrast changes were found to disagree with the rule given by Menzel-Kopp.

Displaced-line* segments with displacement ± 400, *i.e.* $\pm 642'$ and $\pm 242'$ in Figs. 2 and 3, correspond to the enhanced segments. The displaced segments appear *inside* the strong 400 band, in contrast to the similar line segments reported by Gjønnes & Watanabe (1966) who observed them *outside* the strong 200 band in MgO.

It should also be pointed out that the enhanced segments on the $4n+2,\bar{4},\bar{2}$ lines do not form an envelope. Ordinary envelopes can be seen, however, *e.g.* $4n,8,4$ and $2n+1,\bar{9},\bar{5}$ in Fig. 2 and $2n+1,9,1$ in Fig. 4.

Usually, a displaced-line segment is found to continue into an enhanced segment of an ordinary Kikuchi line, as with $\overline{884}'$ and $\overline{484}$ in Fig. 2 (see Fig. 3). However, in some cases a gap appears where the two segments meet, as between $\overline{242}'$ and $\overline{642}$ or between $\overline{242}$ and $\overline{642}'$.

The 084 line appears to be doubled inside the 400 band. This is a spurious effect, involving lines belonging to different zones and is discussed elsewhere (Gjønnes, Høier & Watanabe, 1968).

Calculations and discussion

Theoretical expressions for Kikuchi line contrast have been given by many authors; those given previously by one of us (Gjønnes, 1966) include the effect of Bragg scattering of the incident beam as well as scattering between the coupled diffuse beams. The general expression consists of many terms belonging to a set of form factors for the diffuse scattering, *viz:* $\langle|f(\mathbf{s})|^2\rangle$, $\langle f(\mathbf{s})f^*(\mathbf{s}+\mathbf{h})\rangle$ *etc.* where $\mathbf{s}$ is the scattering vector and $\mathbf{h}/2\pi$ are reciprocal lattice vectors. However, the present study was focused on such contrast effects which were independent of the diffraction conditions of the incident beam. In general, we have sought to avoid situations where strong Bragg reflexions occur and also tried to stick to cases where the diffuse scattering from the direct beam is much stronger near one of the coupled beams than near to the others. Then the main features in the pattern are given by the $|f(\mathbf{s})|^2$ term. Thickness dependent effects can be neglected, since the specimens were wedge-shaped. For a qualitative comparison with observed patterns we may thus use the simplified contrast expressions:

$$\overline{|S_{\mathbf{oo}}|^2}=\sum_j |S_{\mathbf{oo}}^{(j)}|^2 \quad \text{(deficient contrast)}$$

$$\overline{|S_{\mathbf{ho}}|^2}=\sum_j |S_{\mathbf{ho}}^{(j)}|^2 \quad \text{(excess contrast)},$$

where $S_{\mathbf{ho}}(z)=\sum_j S_{\mathbf{ho}}^{(j)} \exp(i\,\xi_j\, z)$ are the amplitudes of the different beams $\mathbf{h}$ at a distance z below the level where diffuse scattering takes place. The index j denotes the branches of the dispersion surface. ξ_j are the *anpassungen*. The bar denotes the usual thickness average.

Calculations of contrast were carried out on a CDC 3300 computer using a diagonalization method for solution of the dynamical equations. A large number of interacting beams could be handled in this way; it was found by trial, however, that the majority of the observed multiple-beam effects were surprisingly well described by three-beam interactions. Hence, it may be appropriate first to present a qualitative discussion of the contrast based on three-beam interactions.

A thorough analytical discussion of the three-beam case was given by Kambe (1957), who explained observed effects in Kossel-Möllenstedt patterns. In many practical cases one of the three Fourier potentials, $V_{\mathbf{h}-\mathbf{g}}$ connecting the three beams $\mathbf{o}$, $\mathbf{h}$ and $\mathbf{g}$ may be taken to be appreciably larger than the others; in fact, our numerical calculations revealed that qualitative conclusions drawn from this simplified case have quite extensive validity.

The following discussion may be seen as summarizing the results of these calculations, of which examples will be given at the end of this chapter.

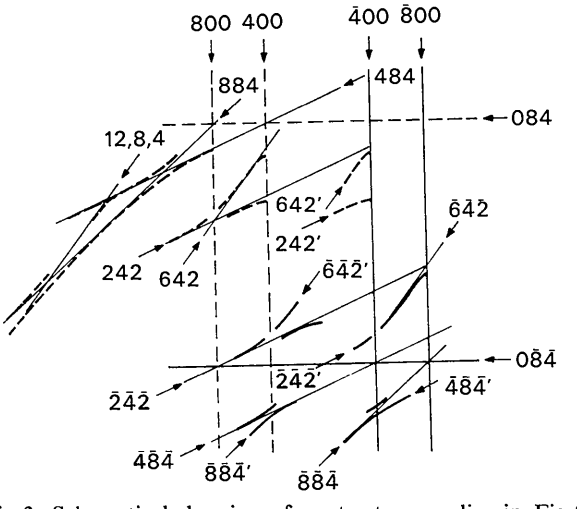

Fig. 3. Schematical drawing of contrast anomalies in Fig. 2. [01$\bar{2}$] zone; for clarity only half the lines are shown.

* The term 'displaced line' was introduced by Gjønnes & Watanabe (1966); their notation, *viz. hkl'* for a displaced line is used below.

A typical three-beam situation is represented in Fig. 5(*a*) which shows three coupled Kikuchi line intersections, T_o, T_g and T_h. The coupling V_{h-g} is assumed to be strong and the other Fourier potentials weak. The Figure thus includes the case of intersecting weak lines with strong coupling between them (T_o) as well as intersections, T_g and T_h, between a weak and a strong line.

The effects of the strong coupling on position and contrast of the weaker lines may profitably be related to the dispersion surface. Fig. 5(*b*) shows a section ($L-L$), near T_g, of the three beam dispersion surface. The three straight lines, **o**, **g** and **g**−**h**, represent spheres with radii equal to the length of the wave vector around each of the reciprocal lattice points **o**, **g** and **g**−**h**. The **o**-beam is taken to be in the vicinity of T_g. The same dispersion surface can, of course, be used in regions near T_o and T_h as well, changing the **o**-line, or free electron sphere, accordingly.

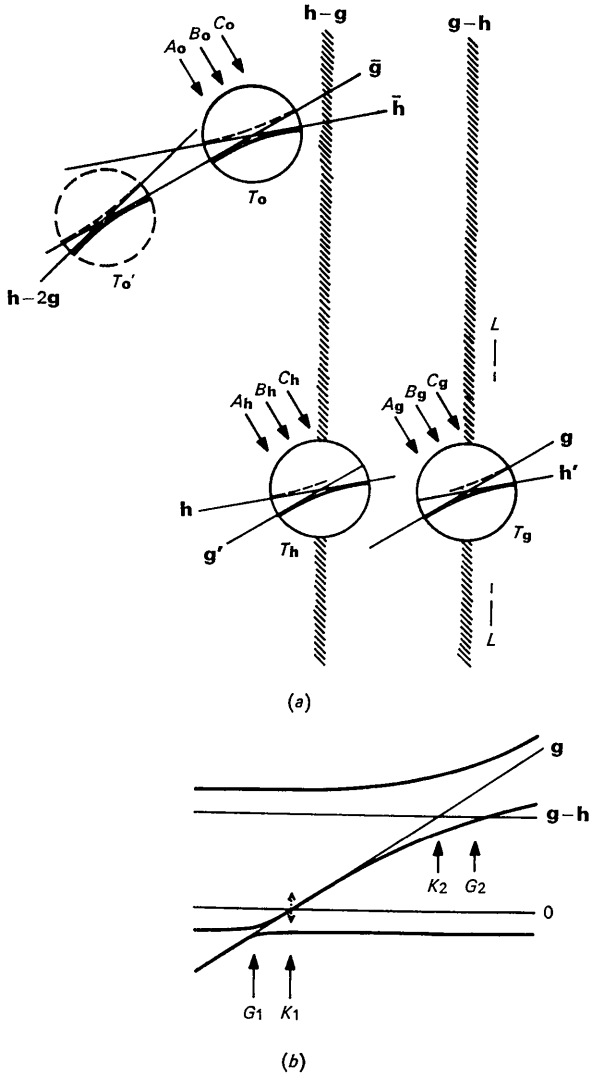

Fig. 5. (*a*) Schematical drawing of enhanced, diminished and displaced line segments in the three-beam case; $P = V_g V_h V_{h-g} > 0$, V_{h-g} is the largest Fourier potential. Enhanced and diminished line segments are shown by heavy and dashed lines, respectively. The sections A_n, B_n and C_n, **n**=**o**, **g**, **h**, indicate the positions of the contrast profiles given in Fig. 8. (*b*) Dispersion surface coresponding to the section *L*–*L*.

Starting with line positions, let us now proceed to a qualitative discussion of three-beam effects near Kikuchi line intersections. The positions of the weaker lines are found to be nearly independent of the weaker potentials and to be given by the intersections between the weak beam spheres [*e.g.* **g** in Fig. 5(*b*)] and the two-beam dispersion surfaces formed by the strong coupling (*i.e.* between **o** and **g**−**h**). In this way G_1 and G_2 indicate the positions of the line **g** and the displaced line **h**', respectively. **h**' – which we might also call an *umweganregung* line – is constructed by translating the line **h** by a vector **g**−**h** (Gjønnes & Watanabe, 1966). The displaced lines are thus related to intersections between the sphere around a weak or moderate reflexion and a strongly excited branch of the dispersion surface, other than the one closest to the free-electron sphere.

From the hyperbolic shape of the two-beam dispersion surface, it follows that the weak lines in the region around T_o will be distorted into two branches of a hyperbola with the two lines $\bar{\mathbf{g}}$ and $\bar{\mathbf{h}}$ as asymptotes – one of which is more strongly excited, as we shall see. This is reflected in the other intersections as hyperbolae with one line and one displaced line, *e.g.* **g** and **h**' at T_g, as asymptotes. Frequently the displaced line segment is quite short and appears only as a tail to the enhanced part of the weak line at the intersection. An example can be seen at the $7\bar{3}\bar{1}$,511 intersection in Fig. 1. Actually, there are two tails which can just be seen to approach the direction of the $2\bar{4}\bar{2}$ line. Here 511 is the coupling reflexion; the existence of tails along the displaced line on both sides of 511 can be explained from the sizes of the Fourier potentials. The more extensive displaced segments shown in Figs. 2 and 3 are pointed out in the previous section.

The above discussion of line position is independent of sign and size of the smaller Fourier coefficients V_g and V_h. However, the contrast of the lines is strongly influenced by these factors. Let us now turn to this question.

In the two-beam case the contrast, or width, of a Kikuchi line is determined by the Fourier potential V_h and is thus related to the gap width, or minimum distance, between the branches of the dispersion surface. Extensive calculations have shown this to be the case also when more beams are excited (see Fig. 9) and here we shall discuss line contrast in such situations in terms of this gap. Referring again to Fig. 5(*b*), one sees that of the two gaps, which in the absence of the strong coupling V_{h-g} would be $2V_g$ and $2V_h$ respectively, one is reduced, G_1, and the other is enhanced, G_2, relative to the two beam values. The situation in Fig. 5(*b*), with the increased gap at the upper branch is obtained when the product $P = V_h V_g V_{h-g} > 0$. When

$P<0$ the situation is reversed, with the increased gap appearing at the lower branch [Fig. 6(*b*)].

In this way the contrast anomalies indicated in Fig. 5(*a*) are readily explained; note that the dispersion surface, [Fig. 5(*b*)] can be used also inside the $\mathbf{h}-\mathbf{g}$ line, near $T_{\mathbf{h}}$, and near the $\bar{\mathbf{g}},\bar{\mathbf{h}}$ intersection, $T_{\mathbf{o}}$.

The contrast of the displaced line can also be predicted. This contrast depends on two factors, *viz*: the particular branch which produces the line must be appreciably excited and there must be an increased gap associated with the displaced line. When the coupling potential $V_{\mathbf{h}-\mathbf{g}}$ is strong, both of these conditions can be satisfied. Fig. 5(*b*) shows an increased gap at G_2 indicating that the displaced line $\mathbf{h}'$ will appear with appreciable contrast outside the $\mathbf{g}-\mathbf{h}$ line. Conversely no displaced line is expected at the inside of line $\mathbf{g}-\mathbf{h}$.

The contrast anomalies near $T_{\mathbf{g}}$ and $T_{\mathbf{h}}$ in Fig. 5(*a*) follow from the discussion above. Note that the enhanced hyperbola branches with one Kikuchi line and one displaced line as asymptotes will have the same type of contrast – excess or deficient. The complemententary nature of contrast thus leads to enhanced contrast for one branch of the corresponding hyperbola near $T_{\mathbf{o}}$ and reduced contrast for the other branch, as shown in Fig. 5(*a*). The contrast in this region can, of course, also be deduced from a dispersion surface construction similar to Fig. 5(*b*), but with the **o**-line shifted to the **g**-line position. Two examples of contrast changes at intersections between weak and strong lines are seen in Fig. 1; the product $P=V_{7\bar{3}1}V_{2\bar{4}2}V_{511}$ or $V_{9\bar{7}3}V_{4\bar{8}4}V_{511}$ is in both cases positive.

When the product P is less than zero, the conditions for enhancement and reduction of contrast are reversed and become as shown in Fig. 6. $P<0$ applies for several three-beam cases as seen in Fig. 2. From the symmetry of the spinel structure it follows that $V_{642}V_{242}V_{400}<0$, hence displaced $\pm 642'$ and $\pm 242'$ lines appear *inside* the 400 band. These segments are coupled to enhanced segments of the ± 642 and ± 242 lines outside the band.

We can now formulate rules for the occurrence of the enhanced or reduced contrast and for the appearance of displaced line segments in three-beam cases.

If the product $P=V_{\mathbf{g}}V_{\mathbf{h}}V_{\mathbf{h}-\mathbf{g}}>0$, a line **g** will appear with enhanced contrast at the side of the strong line $(\mathbf{g}-\mathbf{h})$ where the excitation error $\zeta_{\mathbf{g}-\mathbf{h}}$ is negative and with reduced contrast at the other side of the $(\mathbf{g}-\mathbf{h})$ line. A displaced $\mathbf{g}'$ line segment will appear at the side of the strong line $(\mathbf{h}-\mathbf{g})$ where $\zeta_{\mathbf{h}-\mathbf{g}}$ is positive.

If $P<0$, the line **g** will appear with enhanced contrast at the side of $\mathbf{g}-\mathbf{h}$ where $\zeta_{\mathbf{g}-\mathbf{h}}$ is positive and with reduced contrast where $\zeta_{\mathbf{g}-\mathbf{h}}$ is negative. The displaced $\mathbf{g}'$ segment will then appear where $\zeta_{\mathbf{h}-\mathbf{g}}$ is negative.

These rules and their relation to the gap widths of the dispersion surface have been substantiated experimentally and theoretically in a number of three-beam cases; the qualitative predictions are often borne out even when more interacting beams are present.

Whereas the nature of the contrast anomalies is determined by the signs of the Fourier potentials involved, the magnitude of the effects depends on the relative sizes of the potentials. On varying the Fourier potentials in our calculations of dispersion surfaces and contrast profiles, we have found that the change in contrast of a line **g** on crossing a strong line $\mathbf{g}-\mathbf{h}$ depends on $V_{\mathbf{h}}$. For a given $V_{\mathbf{g}-\mathbf{h}}$, the effect on the line **g** will increase with increasing $V_{\mathbf{h}}$. For a sufficiently strong $V_{\mathbf{h}}$, the split at the intersection will disappear. The intersection $7\bar{3}1,511$ in Fig. 1 is typical of a small $V_{\mathbf{h}}$ $(\mathbf{h}=2\bar{4}2)$. Here the reduced branch of the $7\bar{3}1,2\bar{4}2'$ hyperbola is also seen, so that a split intersection appears. At the $9\bar{7}3,511$ intersection no such split occurs as might be expected since $V_{\mathbf{h}}=V_{4\bar{8}4}$ is much larger

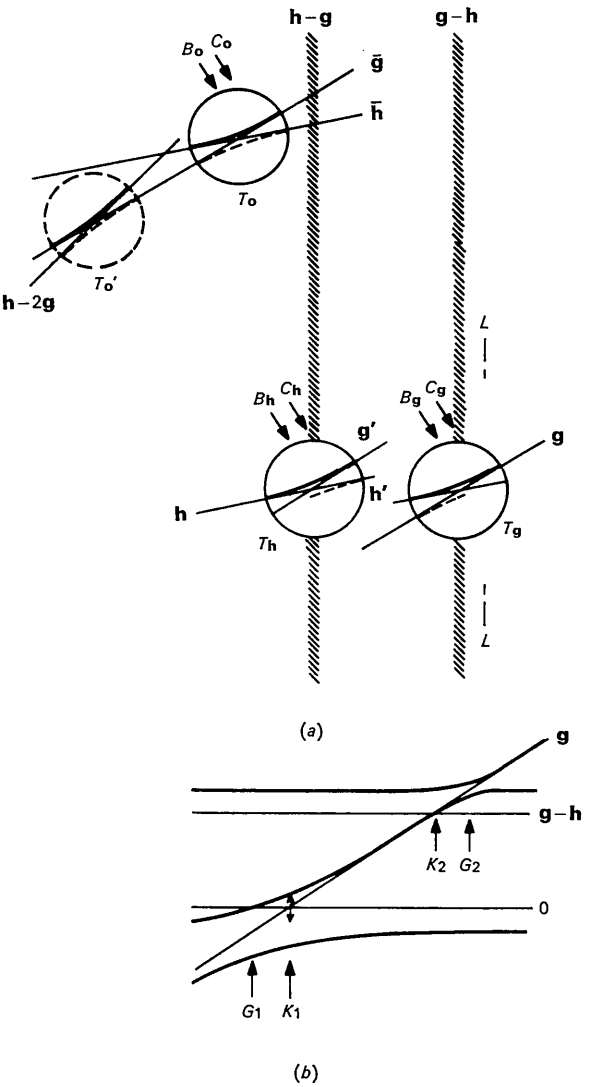

Fig. 6. (*a*) Schematical drawing of enhanced, diminished and displaced line segments in the three-beam case for $P<0$. Enhanced and diminished line segments are shown by heavy and dashed lines, respectively. The sections $B_{\mathbf{n}}$ and $C_{\mathbf{n}}$, $\mathbf{n}=\mathbf{o}, \mathbf{g}, \mathbf{h}$, indicate the positions of the contrast profiles given in Fig. 10. (*b*) Dispersion surface coresponding to the section *L*–*L*.

than $V_{2\bar{4}\bar{2}}$, the other potentials being of equal size. Another example can be found in the paper of Gjønnes & Watanabe (1966), where *e.g.* the 824 line is missing outside the 002 line, where $V_{\mathbf{h}}=V_{822}$, but is still visible outside $00\bar{2}$ where $V_{\mathbf{h}}=V_{826}<V_{822}$.

Several enhanced segments, especially from lines belonging to a layer line in the reciprocal lattice, may combine to form extensive patterns, like the Kikuchi envelope (Shinohara, 1932). The formation of the envelope is seen from Fig. 5(*a*). Contrast enhancements similar to those appearing at T_0 will appear at the $\mathbf{h},\mathbf{h}-2\mathbf{g}$ line intersection T_0' and so on. In this way the relation between the envelope and the network of lines and displaced lines occurring around a strong band (Gjønnes & Watanabe, 1966) is easily understood.

More complicated envelopes can also be found. The one in Fig. 4 is composed of segments from the $(2n+1,9,1)$ lines. The strong coupling is between every second line, *e.g.* 591 and 191 through 400, since 200 is forbidden. In this case the Fourier potentials are $V_{hkl}>0$ for $hkl=(4n+1,9,1)$, $V_{hkl}<0$ for $hkl=(4n+3,9,1)$ and $V_{hkl}=-V_{\bar{h}kl}$. The structure factor products guiding the strong three-beam interactions are thus all positive. The segments which would have formed the usual envelope are relatively unperturbed, whereas a figure with the same direction of curvature as in the usual case is formed by segments outside the envelope position, *e.g.* on the inside of the 191, 591 intersection. At the inside of this enhanced hyperbola branch a straight, unperturbed 391 segment should appear; this is not well resolved in the pattern, however. The 791 potential is very small, and hence this line is invisible except in a small region near the intersection 791, 391 where it appears with enhanced contrast.

It follows from the discussion in connection with Fig. 6 that the envelope will not appear if the structure factor products, P, are negative. In that case the line segments corresponding to the ordinary envelope are reduced in contrast and strongly enhanced segments will appear outside the envelope. In this way a quite different curved figure, which we suggest may be called an 'inverted envelope', arises. Such a curve can be seen in the pattern of $(4n+2,\bar{4},\bar{2})$ lines in Fig. 2. A schematic drawing is given in Fig. 7.

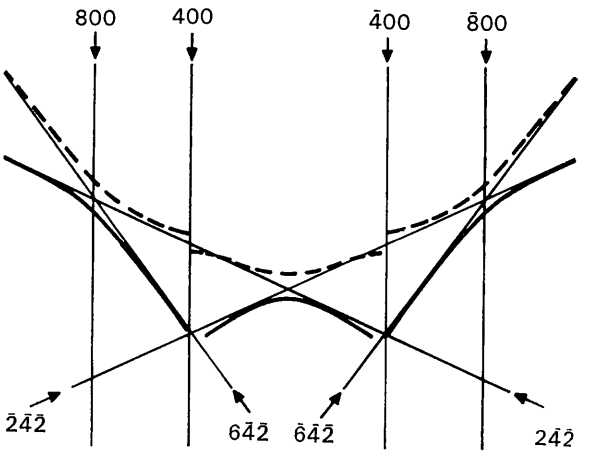

Fig. 7. The 'inverted envelope' formed by the $(4n+2,\bar{4},\bar{2})$ lines in Fig. 2 schematically shown, heavy line. Dashed line: normal envelope position.

The Kikuchi line contrast may, of course, be influenced by interactions involving more than three beams. However, contrast features which depend on four or more beam interactions for their qualitative explanation were found to be relatively infrequent and usually of small extension. An example is the small gap where the $\overline{6}\overline{4}\overline{2}'$ and enhanced $\overline{2}\overline{4}\overline{2}$ meet in Fig. 2; from three-beam considerations alone one would here expect these segments to be joined to form a continuous curve. Contrast calculations for this region are given below.

Let us now consider some examples of numerical calculations relating to the observed contrast anomalies. Fig. 5 may be taken to represent the observed anomalies in Fig. 1, with $\mathbf{g}=7\bar{3}\bar{1}$, $\mathbf{h}=2\bar{4}\bar{2}$, $\mathbf{g}-\mathbf{h}=511$ and with the incident beam near T_0. The relative values of the Fourier potentials $V_{7\bar{3}\bar{1}}, V_{2\bar{4}\bar{2}}, V_{511}$ are approximately -1: -2: 6, $P>0$. A number of contrast profiles were calculated. The profiles reproduced in Fig. 8 correspond to the sections $A_{\mathbf{n}}, B_{\mathbf{n}}$ and $C_{\mathbf{n}}$, $\mathbf{n}=\mathbf{o},\mathbf{g},\mathbf{h}$, indicated in Fig. 5. B_0 is going through the intersection $\mathbf{g},\bar{\mathbf{h}}$ while A_0 and C_0 are at the same distance on each side of this intersection. The profiles of the weak $\pm 7\bar{3}\bar{1}$ lines should be noted especially. These lines appear with enhanced contrast inside the $2\bar{4}\bar{2}$ and 511 bands (A_0 and $A_{\mathbf{g}}$ in Fig. 8) and diminished contrast outside these bands (C_0 and $C_{\mathbf{g}}$). The displaced lines are very weak and the two maxima in the split $7\bar{3}\bar{1}$ line are less well resolved than in the $2\bar{4}\bar{2}$ line, in agreement with the observations in Fig. 1.

These anomalies in Kikuchi line contrast and position can all be inferred from the corresponding dispersion surface, Fig. 8(*d*), as outlined earlier in this section. The simple relation between gap width at the dispersion surface and line contrast, as given by the half width, was tested by calculations performed for various combinations of Fourier potentials for sections of the type A and C. The results, which are summarized in Fig. 9, may be taken as supporting the use of an effective Fourier potential, dependent on the excitation error of the simultaneously excited beam, in a two beam treatment.

The dashed curves for $7\bar{3}\bar{1}$ contrast in Fig. 8 were calculated for opposite sign of $V_{7\bar{3}\bar{1}}$ corresponding to $P<0$. The effect of this change in sign is seen to be a reversal of the contrast anomalies with respect to the 511 line.

Introduction of more beams in the calculations, *e.g.* $4\bar{8}\bar{4}$ and 511, gave only small effects on the contrast profiles.

The contrast variation along the $9\bar{7}\bar{3}$ line in Fig. 1 is explained in a similar way. This line is not split at the intersection with 511. Calculations in which

the sizes of the potentials were varied showed this to be due to the strength of the $48\bar{4}$ reflexion relative to $9\bar{7}3$.

Of the multiple-beam effects in Fig. 2 we present some calculations concerning the central part of Fig. 3. In this case T_0 (Fig. 6) can be taken to represent the area near the 642, 242, 800 triple intersection. Three-beam calculations were performed with $\mathbf{g}=\bar{6}\bar{4}2$, $\mathbf{h}=\bar{2}\bar{4}2$ and $\mathbf{g}-\mathbf{h}=\bar{4}00$. The relative values of the Fourier potentials in this case are $V_{642}:V_{242}:V_{400}\simeq -1:1{\cdot}25:8$, $P>0$. The sections B_0 and C_0 in Fig. 6 are both normal to the $\bar{\mathbf{g}}$ line and intersect this line outside the $\bar{\mathbf{h}}$ line, as indicated in the Figure.

The calculated three-beam profiles given by heavy lines in Fig. 10 correspond to the sections indicated by $B_\mathbf{n}$ and $C_\mathbf{n}$, $\mathbf{n}=\mathbf{o},\mathbf{g},\mathbf{h}$, in Fig. 6. The enhancement of the ± 642 lines outside the 242 and 400 bands seen in the profiles C_0 and $C_\mathbf{g}$ agrees with the observed pattern. The weak tail of the diminished branch of the $\bar{6}\bar{4}2, \bar{2}\bar{4}2$ hyperbola indicated by the calculated profile $C_\mathbf{g}$ could not be observed on the plates, possibly because of other contrast details in this region. In $C_\mathbf{h}$ the diminished $\bar{2}\bar{4}2$ profile and the strong $\bar{6}\bar{4}2'$ displaced line, corresponding to the enhanced $\bar{6}\bar{4}2$ segment, are in qualitative agreement with the observations in Fig. 2.

The effect of four-beam interactions, *i.e.* including 800, can be seen from the dashed curves in Fig. 10. 800 has some influence on both the position and line width in $C_\mathbf{g}$ and $C_\mathbf{h}$, making the enhanced and displaced line segments more pronounced. The large difference between three- and four-beam profiles in Fig. 10(*a*) is a result of the 800 deficient profile. The $\bar{8}00$ excess profile is not shown.

In the sections $B_\mathbf{n}$ the three-beam treatment breaks down completely, as can be seen in the contrast profiles in Fig. 10. The contrast of those branches of the $\bar{2}\bar{4}2$,

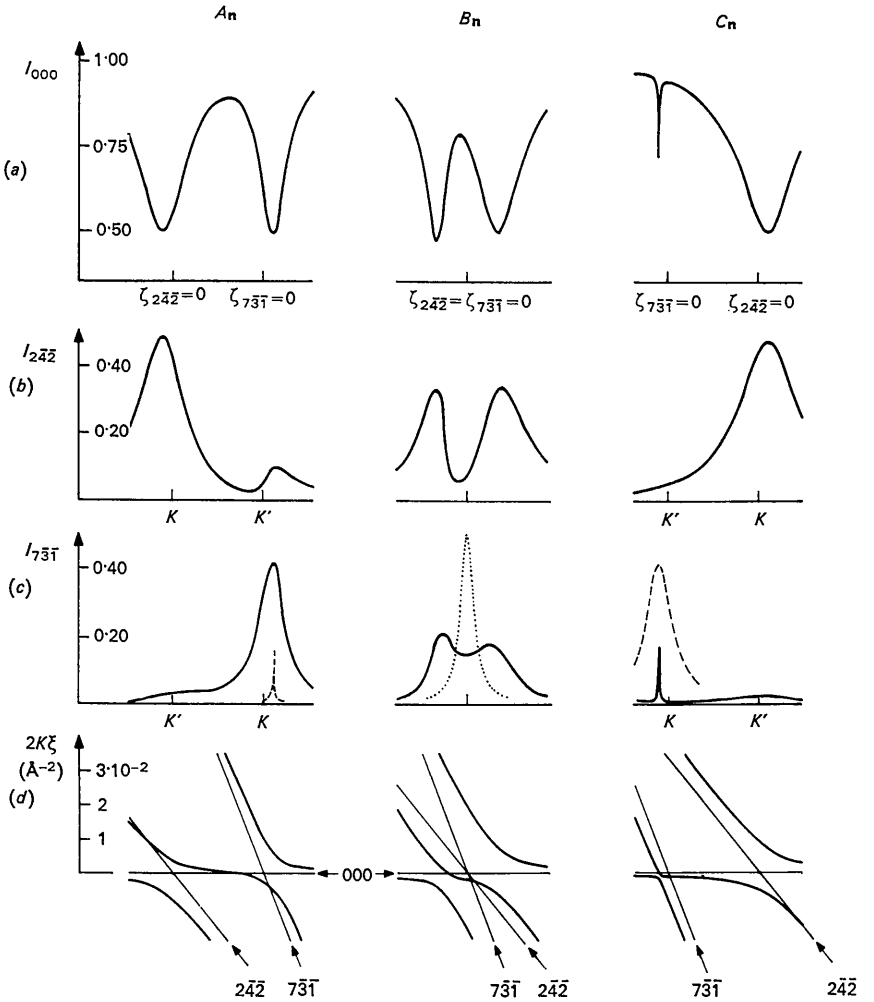

Fig. 8. Calculated contrast profiles $A_\mathbf{n}$, $B_\mathbf{n}$, $C_\mathbf{n}$, $\mathbf{n}=\mathbf{o},\mathbf{g},\mathbf{h}$ (Fig. 5), corresponding to the encircled areas of Fig. 1, $P>0$. K and K' denote geometrical positions of the Kikuchi line and displaced line, respectively. (*a*) Deficient contrast profiles, $\mathbf{n}=\mathbf{o}$. (*b*) $2\bar{4}\bar{2}$ excess profiles, $\mathbf{n}=\mathbf{h}$. (*c*) $7\bar{3}\bar{1}$ excess profiles, $\mathbf{n}=\mathbf{g}$. The dashed curves correspond to $P<0$; dotted curve: two-beam profile. (*d*) Calculated dispersion surface.

$\overline{642}'$ and $\overline{642}, \overline{242}'$ hyperbolae, which according to the three-beam calculations should be strongly enhanced, is seen to vanish almost completely through four-beam interactions. The effects on the dispersion surface, Fig. 10(*d*), are also drastic, the corresponding gap becoming very small. This four-beam effect can be seen in Fig. 2 as a disappearance of contrast between the $\overline{642}$ line and $\overline{242}'$ displaced line near the intersection with the $\bar{4}00$ line, and similarily between the $\overline{242}$ line and $\overline{642}'$ displaced line near the 400 line. Adding further beams, *e.g.* $\bar{4}00$ and $\overline{484}$, in the calculation had little influence on the profiles in Fig. 10.

Conclusions

A number of multiple-beam effects in Kikuchi patterns were studied in the present work, particularly enhancement and reduction of line contrast. Most of the cases could be explained, at least in their broad features, from three-beam interactions.

An important aspect of Kikuchi line studies is the insight one obtains into dynamic effects to be expected in other electron diffraction techniques. In particular, because of the wide range of diffraction conditions recorded in one exposure and the elimination of thickness oscillations, such patterns give a very useful picture of the angular extent of the most important dynamic interactions. The wide applicability found here of three-beam considerations appears to support the use of 'dynamic' or 'effective' potential methods (Bethe, 1928; Gjønnes, 1962; Hall & Hirsch, 1965) which are derived from three-beam interactions.

However, our studies have been aimed at explaining gross features rather than obtaining high accuracies. Further, interactions in densely populated reciprocal lattice planes have not been analysed in detail. In such cases a large number of interacting beams must be included, even in an approximate description; three beam considerations will then be of limited value.

Thus, for an approximate description of dynamic interactions on a weak or moderate reflexion, the diffraction conditions may conveniently be divided in three types:

(1) Incident beam near a principal zone axis; here many beams are needed, even for an approximate treatment. The Kikuchi pattern appears with very complicated and often feeble contrast.

(2) Regions where the incident or diffracted beam is fairly close to the Bragg condition for one strong reflexion. Here three-beam interactions often give a satisfactory description. Such regions are easy to identify in Kikuchi patterns.

(3) Two-beam regions, with no strong coupling to other beams and no anomaly in the Kikuchi line contrast.

As is evident from the reproduced patterns, the three-beam regions can be quite extensive; large effects on line contrast – and hence on integrated intensity and extinction distance – are often found at considerable deviations from the Bragg condition for a stronger reflexion. Actually, the effect on Kikuchi line contrast has its maximum at some distance from the exact Bragg condition for a simultaneous reflexion. At the Bragg condition, *i.e.* the condition studied by Hall (1966), the line contrast may be only slightly different from the two beam value, the main effect being a displacement of the line, corresponding to a change in the angular condition for maximum intensity of the weak reflexion. Frequently, a split line occurs at the intersection, corresponding to the doubly peaked rocking curve calculated by Hall.

The strong enhancement or reduction of line contrast occurring at the two sides of a stronger line depends on the sign of the Fourier potentials involved as well as on the sign of the excitation error for the strong reflexion. Hence the three-beam effects can be used to obtain sign relations between structure factors, *e.g.* for reflexions belonging to a layer line.

The three-beam effects will be most pronounced on the weakest reflexion. However, the enhancement or reduction of a weak beam will be accompanied by a corresponding reduction or enhancement in the strong beam. In this way an apparent absorption resulting from weak beams may occur. Especially at some deviation from the strong beam Bragg condition, this effect can be appreciable, even for a quite far out reflexion with a small Fourier potential. Great care should therefore be exercised when microscope contrast or intensity distributions are interpreted in the two-beam approximation. The Kikuchi pattern may serve as a useful guide to conditions approximating two beams.

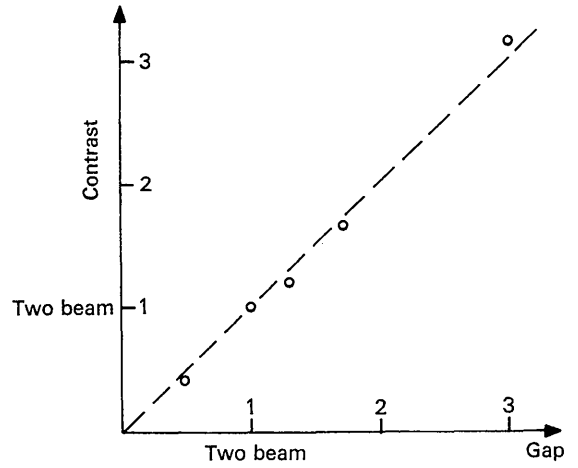

Fig. 9. Calculated contrast in the three-beam case as a function of the perturbed two beam gap corresponding to sections of the type A_n and C_n in Figs. 5 and 8.

References

BETHE, H. A. (1928). *Ann. Phys.* **87**, 55.
GJØNNES, J. (1962). *Acta Cryst.* **15**, 703.
GJØNNES, J. (1966). *Acta Cryst.* **20**, 240.

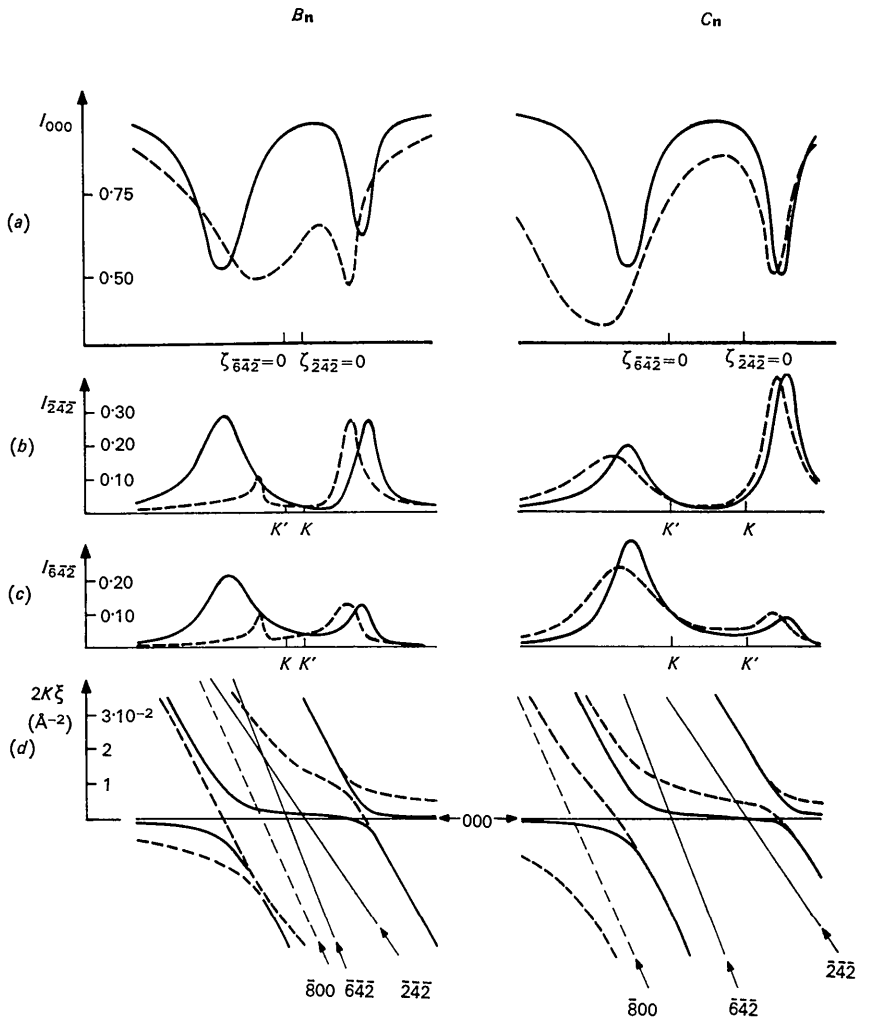

Fig. 10. Calculated contrast profiles B_n and C_n, $n=o,g,h$ (Fig. 6), corresponding to the observed ±642 and ±242 contrast in Fig. 2, $P<0$. Full line: three-beam profiles. Dashed line: Four beam profiles. (*a*) Deficient contrast profiles, $n=o$. (*b*) $\bar{2}4\bar{2}$ excess profiles, $n=h$. (*c*) $\bar{6}4\bar{2}$ excess profiles, $n=g$. (*d*) Calculated dispersion surface.

GJØNNES, J. & WATANABE, D. (1966). *Acta Cryst.* **21**, 297.
GJØNNES, J., HØIER, R. & WATANABE, D. (1968). *Acta Cryst.* A**25**, 300.
HALL, C. R. (1966). *Phil. Mag.* **14**, 155.
HALL, C. R. & HIRSCH, P. B. (1965). *Phil. Mag.* **12**, 539.
HØIER, R. (1969). *Acta Cryst.* A**25**, 516.
KAMBE, K. (1957). *J. Phys. Soc. Japan,* **12**, 13.
MENZEL-KOPP, C. (1962). *J. Phys. Soc. Japan,* B-II, **17**, 76.
PFISTER, H. (1953). *Ann. Phys.* **11**, 239.
SHINOHARA, K. (1932). *Sci. Pap. Inst. Phys. chem. Res. Tokyo,* **20**, 39.
UYEDA, R. (1965). *Acta Cryst.* A**24**, 175.
WATANABE, D., UYEDA, R. & FUKUHARA, A. (1968). *Acta Cryst.* A**24**, 580.